Acta
Materia
Medica

Research Article

Cuproptosis-related MTF1 inhibits kidney renal clear cell carcinoma progression by suppressing proliferation and regulating immune cell infiltration

Graphical abstract

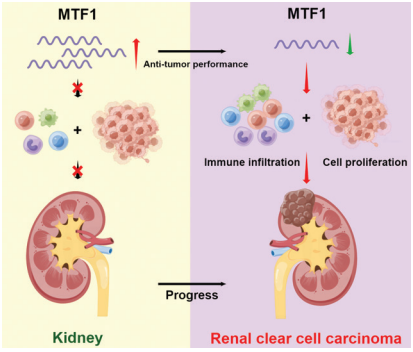

Highlights

- We screened four cuproptosis-related genes (CRGs) in patients with kidney renal clear cell carcinoma.
- MTF1 and FDX1 were identified as two independent overall survival CRGs in patients with kidney renal clear cell carcinoma.
- Knockdown of MTF1 promotes kidney renal clear cell carcinoma by promoting proliferation and modulating immune cell infiltration.

Authors

Weipu Mao, Zhou Ding, Keyi Wang and Ming Chen

Correspondence

mingchenseu@126.com (M. Chen)

In brief

We found that cuproptosis-related MTF1 acts as a tumor suppressor, involved in the progression of kidney renal clear cell carcinoma by promoting proliferation and regulating immune cell infiltration.

https://doi.org/10.15212/AMM-2023-0016
310 Acta Materia Medica 2023, Volume 2, Issue 3, p. 310-322

Acta Materia Medica

Research Article

Cuproptosis-related MTF1 inhibits kidney renal clear cell carcinoma progression by suppressing proliferation and regulating immune cell infiltration

Weipu Mao[a], Zhou Ding[b], Keyi Wang[c,d] and Ming Chen[a,*]

[a]Department of Urology, Affiliated Zhongda Hospital of Southeast University, Nanjing 210009, China
[b]Department of Urology, Affiliated Hospital of Kangda College, Nanjing Medical University, Huai'an 223400, China
[c]Department of Medical Oncology, Dana-Farber Cancer Institute, Harvard Medical School, Boston, Massachusetts, USA
[d]Department of Urology, Shanghai Tenth People's Hospital, School of Medicine, Tongji University, Shanghai 200072, China

***Correspondence:** mingchenseu@126.com (M. Chen)

Received: 29 April 2023; Revised: 19 June 2023; Accepted: 5 August 2023

Published online: 22 August 2023

DOI 10.15212/AMM-2023-0016

ABSTRACT

Cuproptosis is a newly identified specific form of programmed cell death. Our study aimed to identify cuproptosis-related genes (CRGs) in patients with kidney renal clear cell carcinoma (KIRC) from the The Cancer Genome Atlas database and to evaluate CRG biological functions. Using lasso regression, we identified four KIRC prognosis-associated CRGs and constructed an associated prognostic risk signature. Kaplan-Meier curves showed that patients with high-risk scores had significantly lower survival times than patients with low-risk scores. Multivariate Cox analysis identified MTF1 and FDX1 as two independent overall survival CRGs. Moreover, qRT-PCR showed that MTF1 and FDX1 expression was downregulated in KIRC and knockdown of MTF1 and FDX1 significantly promoted KIRC cell proliferation and migration ability. In addition, the MTF1 level was positively correlated with immune cell infiltration and knockdown of MTF1 promoted tumor growth *in vivo*. We developed a signature of prognostic risk-associated CRGs that accurately predicted the prognostic status of KIRC patients. MTF1 and FDX1 were shown to be key CRGs. MTF1 acts as a tumor suppressor, and may be involved in the progression of KIRC by inhibiting proliferation and regulating immune cell infiltration.

Keywords: Cuproptosis, Kidney renal clear cell carcinoma, MTF1, Immune cell infiltration

1. INTRODUCTION

Renal cancer is one of the most common urinary tract malignancies originating from renal tubular epithelial cells. Renal cancer accounts for 2.2% of all malignant tumors, with renal clear cell carcinoma (KIRC) the most common type of renal cancer [1, 2]. Currently, the primary treatment for KIRC is surgery, but distant metastases are found at the time of diagnosis in 25%-30% of patients, thus patients may eventually develop recurrent metastatic KIRC even after surgical resection [3]. Surgical treatment for metastatic KIRC is limited, with a 5-year postoperative survival rate < 10% [4]. Moreover, radiotherapy and immunotherapy are not effective for patients with metastasis. Despite many major breakthroughs in the treatment of KIRC with targeted therapies in recent years, the prognosis remains poor [5, 6]. It is of great research and clinical significance to better understand the mechanism underlying KIRC development, to explore diagnostic and therapeutic approaches at the molecular level with multiple genes, and to seek effective targeted therapies.

Metal ions are indispensable trace elements for living organisms, but insufficient or excessive levels of metal ions can cause cell death [7, 8]. Copper, a trace metal, is an important cofactor, the redox properties of which make copper both beneficial and toxic to cells [9, 10]. Recent studies have revealed that copper ionophores are intrinsically selective in preferentially inducing cancer cell cuproptosis [11]. Tsvetkov et al. [12] reported that intracellular copper accumulation leads to a novel type of programmed cell death (PCD) called cuproptosis, and

identified 10 cuproptosis-related genes (CRGs [CDKN2A, DLAT, DLD, FDX1, GLS, LIAS, LIPT1, MTF1, PDHA1, and PDHB]). The correlation between the expression of CRGs and KIRC, however, has not been thoroughly investigated. The establishment of new biomarkers related to cuproptosis is important for the early detection and prognosis of KIRC.

Metal regulatory transcription factor (MTF) 1 is a protein-coding gene that accumulates in the nucleus during heavy metal exposure and activates transcription of metallothionein (MT) genes by binding to the promoter of the metal response element [MRE] [13, 14]. Diseases associated with MTF1 include dentin erosion and enamel erosion [15]. Recently, a growing number of studies have identified that MTF1 has an important role in the progression of a variety of malignancies, including gastric cancer, hepatocellular carcinoma, and prostate cancer [16-18].

Therefore, we first searched for KIRC prognosis-associated CRGs using gene expression profiles from The Cancer Genome Atlas (TCGA) database. Second, a prognostic risk-related signature was developed based on the above CRGs to find novel biomarkers to assess the prognosis of KIRC. Finally, we validated the expression of the above CRGs in tissue samples and cells, and functional experiments were performed to assess the biological functions.

2. MATERIALS AND METHODS

2.1 Data sources and preparation

We obtained transcriptome fragments per kilobase per million (FPKM) data for 538 KIRC and 72 healthy patients from the TCGA database. Log2 (FPKM+1) processing was performed on the data. Clinical information was obtained, including gender, age, grade, pathologic stage, TNM stage, survival status, and survival time (**Table 1**).

Table 1 | Clinical information of 523 KIRC patients in the TCGA.

Characteristics	KIRC patients (N = 523)	No. %
Age, years		
< 65	328	62.72%
≥ 65	195	37.28%
Gender		
Male	338	64.63%
Female	185	35.37%
Tumor		
T1	270	51.6%
T2	66	12.6%
T3	176	33.7%
T4	11	2.1%
Node		
N0	233	44.6%
N1	15	2.9%
NX	275	52.6%
Metastasis		
M0	435	83.2%
M1	88	15.3%
MX	8	1.5%
Stage		
Stage I	264	50.5%
Stage II	54	10.3%
Stage III	122	23.3%
Stage IV	83	15.9%
Grade		
G1	14	2.7%
G2	286	43.2%
G3	206	39.4%
G4	77	14.7%
Vital status		
Alive	363	69.4%
Dead	160	30.6%

2.2 Construction and validation of a prognostic signature associated with CRGs

The 478 samples with a survival time >30 days were randomly divided into training (355 cases) and test sets (143 cases) at a 7:3 ratio. CRGs associated with prognostic risk were screened by least absolute shrinkage and selection operator (lasso) Cox regression. Risk models were subsequently constructed and the clinical samples were divided into low- and high-risk groups. Kaplan-Meier survival curves and Cox proportional risk analysis were used to determine the effect of risk models on overall survival (OS).

2.3 Prognostic nomogram establishment and validation

The OS prognostic nomogram was constructed based on the results of multivariate Cox proportional risk analysis. Calibration curves and receiver operating characteristic (ROC) curves were used to detect the predictive effect of the nomogram, and the results of ROC curves were visualized as the area under the ROC curve (AUC).

2.4 OS-associated independent CRGs

The prognostic risk-related CRGs were subjected to univariate and multivariate Cox regression analyses

to identify the independent CRGs associated with OS. Subsequently, Kaplan-Meier survival curves were used to assess the different levels of CRG expression for the detection of 5-year survival and OS in KIRC patients.

2.5 Clinical samples

We collected tumor and normal tissues from 25 KIRC patients who underwent nephrectomy in the Department of Urology of Shanghai Tenth People's Hospital (Shanghai, China) and the Affiliated Zhongda Hospital of Southeast University (Nanjing, China) from February 2018 to October 2019. The histopathology of all KIRC cases was confirmed by senior pathologists. The methodology of this study was conducted in accordance with the Declaration of Helsinki and approved by the Ethics Committee and Institutional Review Board of Shanghai Tenth People's Hospital (SHSY-IEC-4.1/19-211/01). All patient or their relatives were informed of the study protocol.

2.6 Cell lines and culture

Normal renal tubular epithelial cells (HK-2, catalog number SCSP-511) and human KIRC cell lines (786-O, catalog number SCSP-5059; ACHN, catalog number SCSP-5063; and Caki-1, catalog number SCSP-5064) were purchased from the Cell Bank of the Chinese Academy of Sciences (Shanghai, China). The medium and culture conditions used to maintain each cell line were performed as previously described [2]. The KIRC cell lines were stored at –80°C using Cellsaving reagent (NCM, Suzhou, China).

2.7 Cell transfection

Negative control (si-NC), si-MTF1#1, si-MTF1#2, si-FDX1#1, and si-FDX1#2 were purchased from RiboBio (Guangzhou, China). Cells were transfected using Liposomal Transfection reagent (Yeasen, Shanghai, China) at a cell confluency of 30%-50%. Control lentivirus (sh-NC) and knockdown lentivirus (sh-MTF1) were purchased from IBSBIO (Shanghai, China). The 786-O cells were plated in 24-well plates at 1×10^5 cells/well. When the cells reached 50% growth, the medium was replaced with 2 ml of fresh medium containing 6 μg/ml of polybrene, and an appropriate amount of virus suspension was added. After incubation at 37°C for 4 h, 2 ml of fresh medium was added to dilute the polybrene, the cell cultures were continued, and puromycin was used to screen for stable, transfected cells.

2.8 qRT-PCR

Total RNA was extracted from cells or tissue specimens using a tissue grinder (JXFSTPRP-CLQL-48; Jingxin, Shanghai) and Trizol reagent (TaKaRa, China). cDNA was obtained by reverse transcription using a cDNA kit (Vazyme Biotech, Nanjing, China) and subsequently subjected to qRT-PCR. The CT values of the samples were determined using a qRT-PCR detection system (Applied Biosystems, USA). The relative expression of MTF1 and FDX1 was determined using the $2^{-\Delta\Delta Ct}$ method. Information on all primers are as follows: MTF1-F, 5′ ACCCTGGCACTTTGGAGGAT 3′; MTF1-R, 5′ GCTGCACATAACCCTGGGAC 3′; FDX1-F, 5′ CTTTGGTGCATGTGAGGGAA 3′; FDX1-R, 5′ GCATCAGCCACTGTTTCAGG 3′; GAPDH-F, 5′ AACGGATTTGGTCGTATTG 3′; and GAPDH-R, 5′ GGAAGATGGTGATGGGATT 3′.

2.9 Cell Counting Kit-8 (CCK-8) assay

Transfected cells at a density of 2000 per well were seeded in 96-well plates (Corning, USA). After incubation for 0, 24, 48, 72, and 96 h, the media were discarded and replaced with 110 μl of a mixed solution (10 μl of CCK-8 solution; Yeasen, Shanghai, China and 100 μl of serum-free medium). The optical density (OD) values were measured at 450 nm using a microplate spectrophotometer (BioTek, Winooski, USA) after a 2-h incubation.

2.10 EdU assay

Transfected cells were inoculated in 6-well plates (Corning). Cells were fixed after incubation with 10 μM of EdU solution (RiboBio) for 2 h. The cells were washed with PBS after cell permeabilization. Next, the cells were incubated in the dark with Apollo, the nuclei were counterstained with Hoechst, and images were obtained with a microscope.

2.11 Wound healing assay

The treated cells were scored with a 200-μl pipette tip when 80% confluence was reached in a 6-well plate (Corning). The debris was washed off with PBS, and media containing 2% fetal bovine serum (FBS) was added to each well. Images were obtained using an Olympus microscope (Tokyo, Japan) 0 and 24 h after making the wound.

2.12 Immune infiltration analysis

Immune infiltration analysis was performed as previously reported [19]. MTF1 and FDX1 were analyzed in relation to 22 types of immune cells using the Tumor Immune Estimation Resource (TIMER; https://cistrome.shinyapps.io/timer/) database and Xiantao (https://www.xiantao.love/) software.

2.13 Immunohistochemistry (IHC)

The IHC analysis consists of two parts. The level of FDX1 and MTF1 protein expression in tumor and normal tissues were acquired from The Human Protein Atlas (HPA) database (https://www.proteinatlas.org/). Fresh tumor tissues were obtained from mice, fixed in 4% paraformaldehyde, and stained by IHC according to a previous protocol [2].

2.14 Xenograft tumor model

Ten male BALB/c-nu mice, 4-6 weeks old, were purchased from Slac Laboratory Animal Center (Shanghai, China). Mice were randomly divided into two groups and housed in an SPF environment. Mice were injected in the back

with 1 × 10^6 sh-NC and sh-MTF1 stable transgenic cells. The length and width of the tumors were measured weekly. The tumor volume was calculated using the following formula: volume (mm^3) = 0.5 × $width^2$ × length. After sacrificing the mice, the weights of each tumor from all mice were recorded. All animal experiments were performed in accordance with the protocol approved by the Animal Research Ethics Committee of the Shanghai Tenth People's Hospital (SHDSYY-2021-1726).

2.15 Statistical analysis

A $\chi 2$ test or two-tailed Student's t-test were used to calculate the differences between components. Univariate and multivariate Cox regression models were used for survival analyses. R-Studio statistical (Boston, MA, USA) and GraphPad Prism 8.3 software (San Diego, CA, USA) were used in this study. P values were considered statistically significant at <0.05.

3. RESULTS

3.1 Construction and validation of prognostic signature associated with CRGs

Applying lasso Cox regression, four CRGs (CDKN2A, FDX1, LIAS, and MTF1) associated with prognostic risk were identified (Figure 1a). We developed a risk model based on the above four CRGs of the lasso regression analysis described above and divided the clinical samples into low- and high-risk groups in the training and test sets. The scatter plot of risk scores and heat map showed that survival outcomes were worse in the high-risk score patients than the low-risk score group in both the training and test sets (Figure 1b, c). Kaplan-Meier survival analysis showed that patients in the high-risk score group had a significantly lower OS than the low-risk score group (training dataset: P<0.001; test dataset: P=0.043; Figure 1d). Subsequently, univariate and multivariate Cox regression analyses showed that risk model, pathologic stage, grade, and age were independent prognostic risk factors for OS (Figure 1e, f).

3.2 Prognostic nomogram establishment and validation

In addition, we combined age, grade, stage, and risk model to construct a prognostic nomogram for OS that predicted 1-, 3-, and 5-year survival in KIRC patients (Figure 2a). Calibration curves showed that survival predicted by this OS prognostic nomogram was highly consistent with actual survival (Figure 2b), and the ROC curves showed that the AUCs for 1-, 3-, and 5-year OS were 0.84, 0.79, and 0.76, respectively (Figure 2c). These results indicated that the constructed OS prognostic nomogram had high reliability and accuracy.

We then evaluated the prognostic impact of the four CRGs on 5-year survival and OS in the KIRC patients. Kaplan-Meier curves showed that higher levels of FDX1, LIAS, and MTF1 expression were positively associated with better 5-year survival and OS, while high CDKN2A expression was negatively associated with 5-year survival (Figure 2d, e). Correlation studies between the four CRGs showed a strong correlation between MTF1 and FDX1 and LIAS, and between LIAS and FDX1 (Figure 2f). We performed multivariate Cox analysis and found that FDX1 and MTF1 were independent CRGs associated with OS (Figure 2g).

3.3 Expression of FDX1 and MTF1 in TCGA-KIRC database

We examined the relative levels of FDX1 and MTF1 expression in TCGA-KIRC clinical samples, and the relationship between FDX1 and MTF1 expression and clinicopathologic variables. We first determined the level of FDX1 expression. FDX1 expression was downregulated in tumors (Figure 3a), and the downregulation of FDX1 expression was validated in the GSE16449 dataset (Figure 3b). In addition, the HPA database showed that FDX1 protein was downregulated in renal cell cancer tumor tissue (Figure 3c). Furthermore, FDX1 expression were correlated with T-stage, N-stage, M-stage, histologic grade, and pathologic stage (Figure 3d-h). Similarly, FDX1 expression was downregulated in the TCGA database and the GSE16449 dataset (Figure 3i-j), and the HPA database showed that FDX1 protein was downregulated in RCC tumor tissue (Figure 3k). Furthermore, MTF1 expression was associated with T-stage, histologic grade, and pathologic stage (Figure 3l-p).

3.4 Knockdown of FDX1 and MTF1 promoted the proliferation and migration of KIRC cells

qRT-PCR assays showed that MTF1 and FDX1 expression was downregulated in KIRC cell lines (Figure 4a), and MTF1 and FDX1 mRNA expression was reduced in tumor samples (Figure 4b). We designed two siRNAs each for MTF1 and FDX1. qRT-PCR showed that si-MTF1#2 and si-FDX1#2 better reduced MTF1 and FDX1 expression (Figure 4c). CCK-8 and EdU assays showed that knockdown of MTF1 or FDX1 expression significantly promoted the proliferation of 786-O cells (Figure 4d, e). The wound healing assay showed that silencing MTF1 or FDX1 enhanced the migration ability of 786-O cells (Figure 4f).

3.5 MTF1 levels positively correlated with immune cell infiltration

An increasing number of studies in recent years have reported that immune cell infiltration is associated with tumor progression. We then analyzed the correlation between FDX1, MTF1, and tumor infiltrating immune cells. MTF1 was negatively correlated with cytotoxic cells and Tregs. MTF1 was positively correlated with Th1 cells, Th2 cells, dendritic cells (DCs), iDCs, natural killer (NK) cells, macrophages, Tgd, Tem, mast cells, neutrophils, eosinophils, T helper cells, and Tcm (Figure 5a, b). In contrast, FDX1 was negatively correlated with Tregs, cytotoxic cells, aDCs, T cells, pDCs, Tem and CD8 T cells. FDX1 was positively correlated with iDCs, eosinophils, mast

Acta Materia Medica

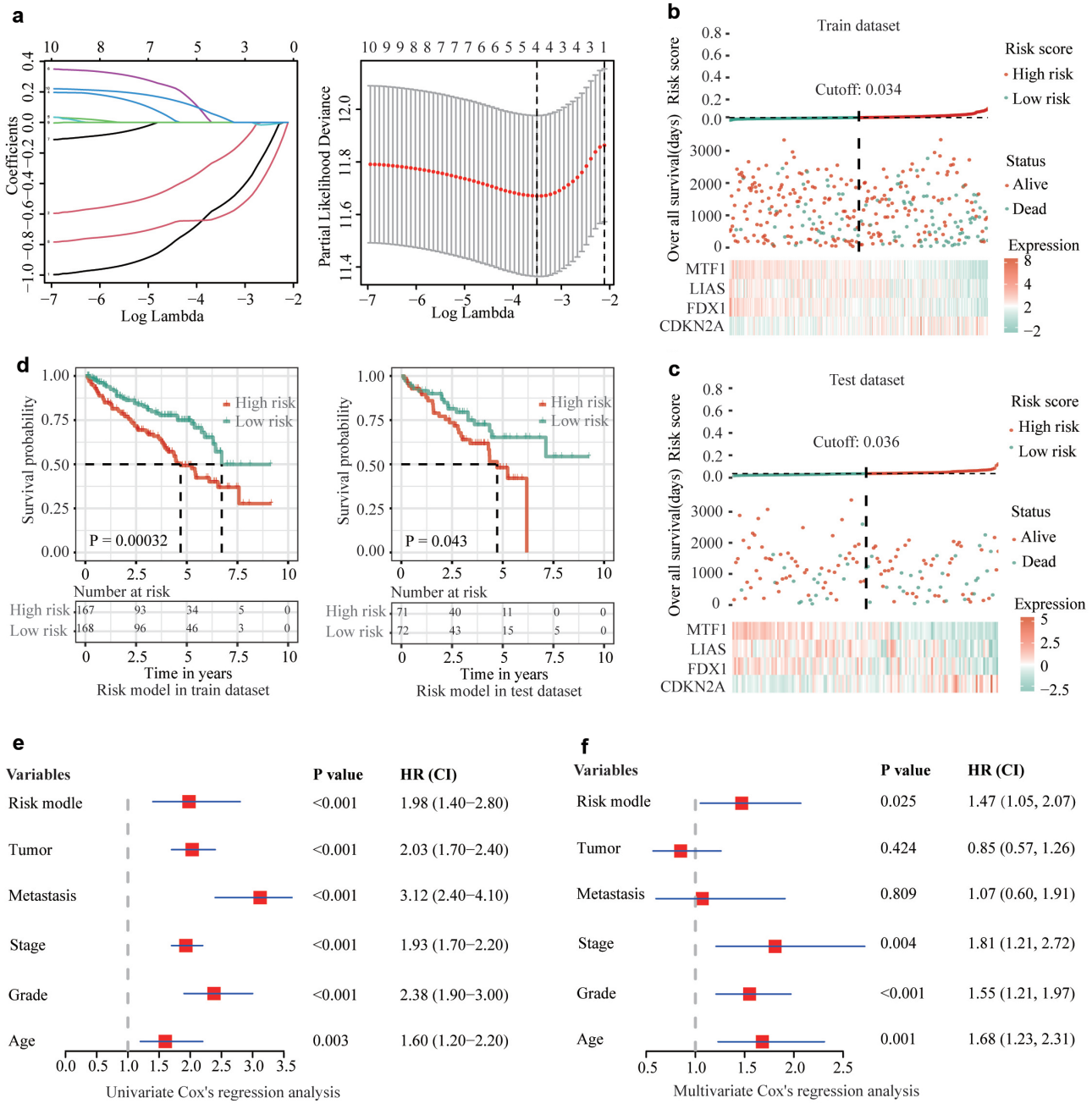

Figure 1 | Construction and validation of prognostic signature associated with CRGs to predict KIRC prognosis.
a. Lasso coefficient profiles and the best log (lambda) value of the prognostic CRGs. **b, c**. The high- and low-risk score distribution in the training (**b**) and test groups (**c**). **d**. Kaplan–Meier survival curve for KIRC patients with high- and low-risk scores in the training and test groups. **e**. The forest plots for univariate Cox regression analysis showed that risk model, tumor, metastasis, stage, grade, and age were prognostic risk-related variables. **f**. The forest plots for multivariate Cox regression analysis showed that risk model, stage, grade, and age were independence prognostic risk-related variables.

cells, neutrophils, and Tgd (Figure S1a, b). Furthermore, MTF1 expression had a strong positive correlation with B cells, CD8+ T cells, CD4+ T cells, macrophages, neutrophils, and DCs (Figure 5c). FDX1 expression had a weak positive correlation with B cells, macrophages, and neutrophils (Figure S1c).

3.6 Knockdown of MTF1 promoted tumor growth *in vivo*

We subsequently determined the *in vivo* function of MTF1 using a xenograft tumor model. Knockdown of MTF1 significantly increased tumor growth, volume, and weight in mice (Figure 6a-d), and the IHC results of

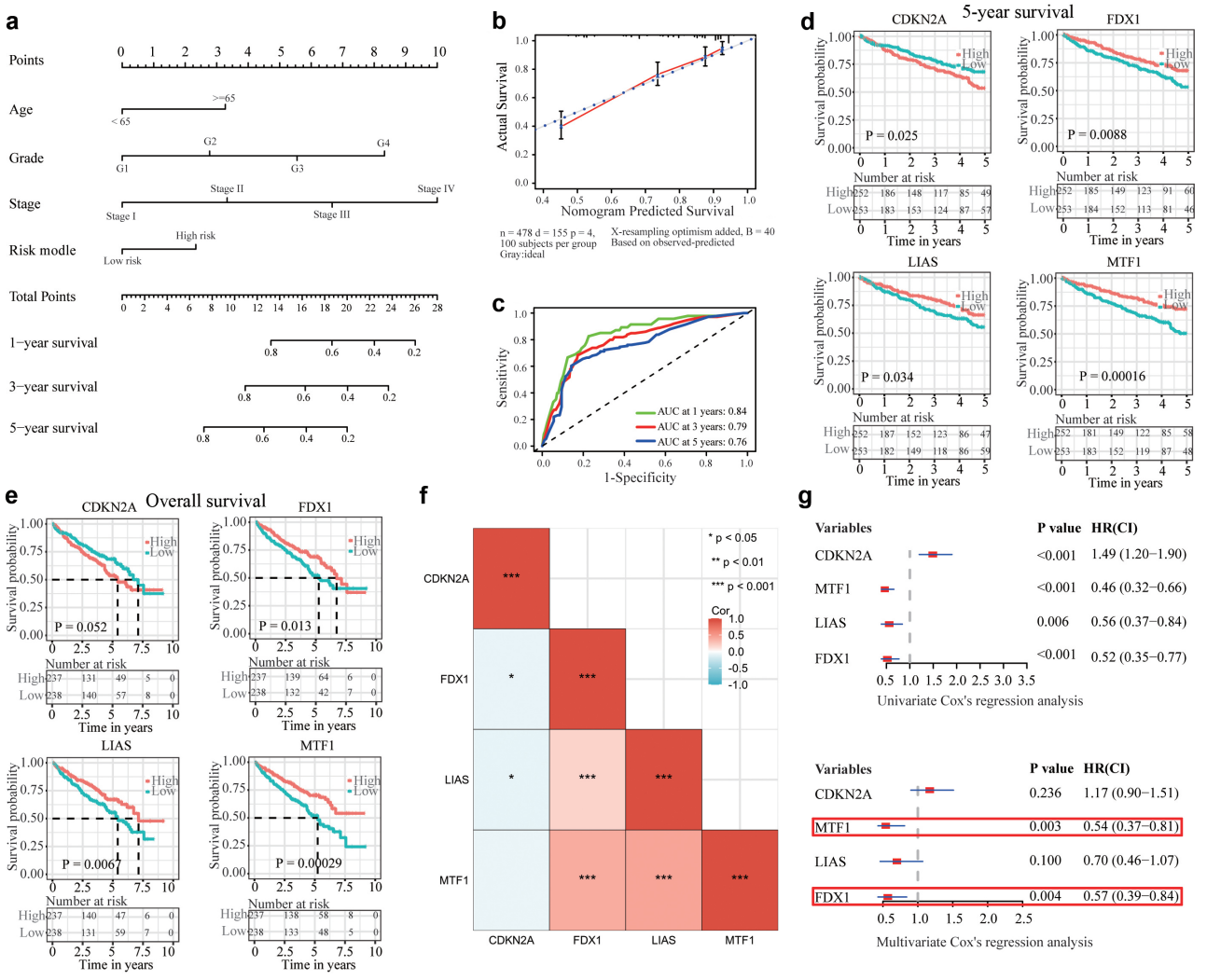

Figure 2 | Establishment of a nomogram based on clinicopathologic characters including risk model.
a. Prognostic nomogram for KIRC patients were constructed based on risk models and other prognosis-related clinicopathologic variables. **b**. Calibration curves for nomograms showed agreement between predicted and actual survival. **c**. ROC curves showed that prognostic nomograms were better able to predict 1-, 3-, and 5-year overall survival in KIRC patients. **d.** The 5-year survival rate of KIRC patient with high or low 4 CRG expression. **e**. The overall survival rate of KIRC patients with high or low 4 CRG expression. **f**. Correlation between the four CRGs in the TCGA database. **g**. Univariate and multivariate Cox regression analysis of overall survival related to KIRC patient CRGs.

Ki67 and MTF1 were confirmed (Figure 6e). The above results suggest that MTF1 has an important role as a tumour suppressor in KIRC progression.

4. DISCUSSION

In this study we first examined the expression of 10 CRGs in the TCGA-KIRC database, identified 4 prognosis-associated CRGs (CDKN2A, FDX1, LIAS, and MTF1) using lasso Cox regression analysis, and constructed prognostic risk-related signatures. Subsequently, a prognostic nomogram for OS containing the p risk model was constructed, and two independent CRGs (FDX1 and MTF1) for OS were screened. Finally, the relative expression of FDX1 and MTF1 were validated in cell and tissue samples. FDX1 and MTF1 expression was downregulated in cell lines and tumor tissues. Knockdown of FDX1 and MTF1 expression promoted the migration and proliferation ability of KIRC cells. In addition, MTF1 expression was positively correlated with immune cell infiltration, and knockdown of MTF1 promoted tumor growth *in vivo*.

PCD is prevalent during the development of living organisms and is a genetically-determined active and ordered method of cell death. Currently, PCD mainly includes apoptosis, autophagy, oncosis, necroptosis, and pyroptosis. Cuproptosis is a new mode of cell death discovered in the last 2 years. Cuproptosis was first

Acta Materia Medica

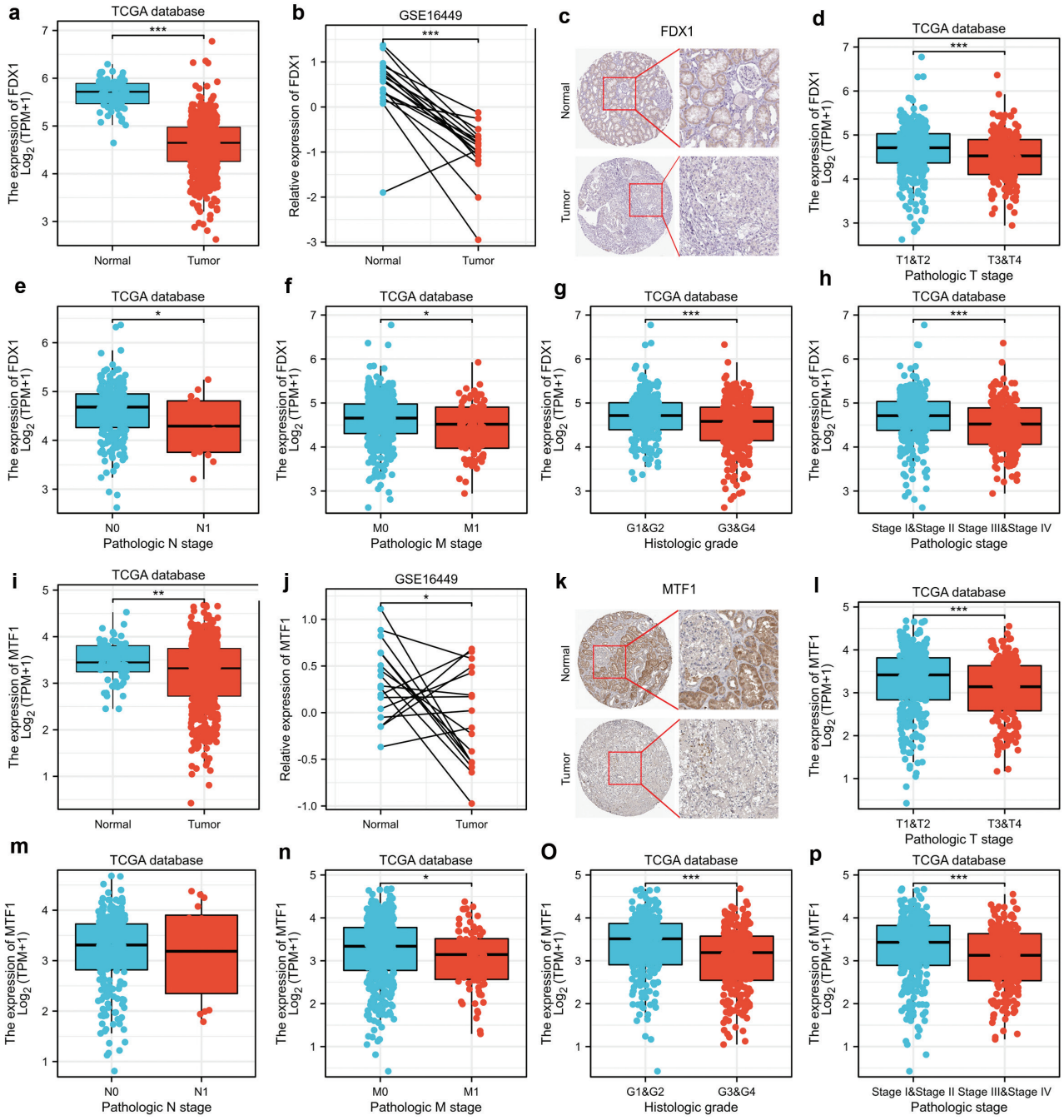

Figure 3 | Expression of FDX1 and MTF1 in the TCGA-KIRC database.
a. FDX1 expression in KIRC and healthy tissues in the TCGA database. **b**. Relative expression of FDX1 in the GSE16449 database. **c**. The levels of FDX1 protein based on the Human Protein Atlas. **d-h**. Relative level of FDX1 expression in the TCGA database with T stage (**d**), N stage (**e**), M stage (**f**), pathologic stage (**g**), and tumor grade (**h**). **i**. MTF1 expression in KIRC and healthy tissues in the TCGA database. **j**. Relative expression of MTF1 in the GSE16449 database. **k**. The level of MTF1 protein based on the Human Protein Atlas. **l-p**. Relative level of MTF1 expression in the TCGA database with T stage (**l**), N stage (**m**), M stage (**n**), pathologic stage (**o**), and tumor grade (**p**). (*p < 0.05, **p < 0.01, ***p < 0.001).

described by Cobine in 2020 as a Cu-elesclomol triggered, ferredoxin-dependent form of cell death [10]. Subsequently, Ge [9] and Oliveri [11] successively reported that copper-based cup cell death has an important role in tumors. Recently, Tsvetkov et al. [12] reported that cuproptosis occurs through direct binding of copper to

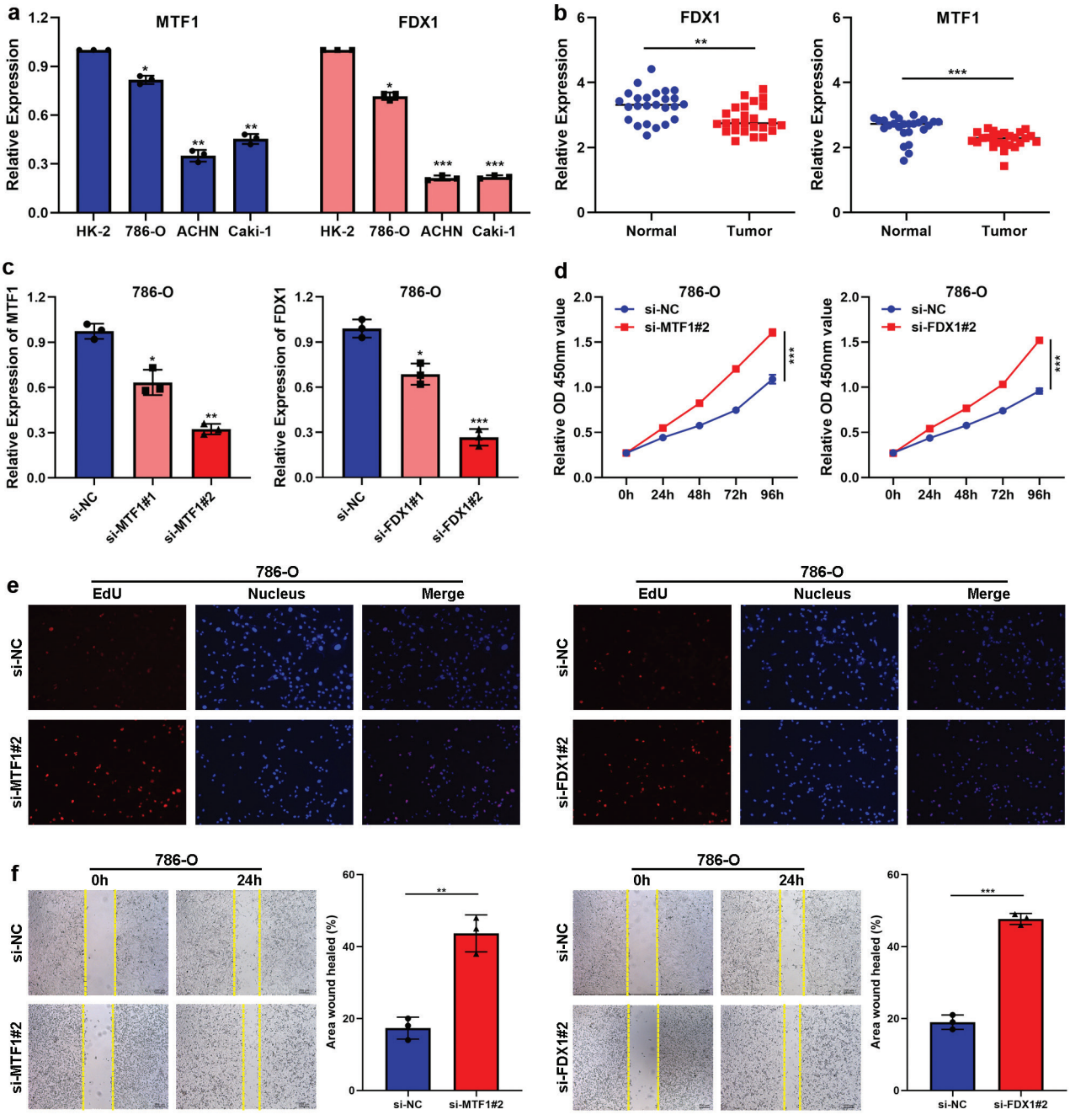

Figure 4 | Knockdown of FDX1 and MTF1 promotes the proliferation and migration of KIRC cells.
a. qRT-PCR analysis of MTF1 and FDX1 expression in KIRC cell lines. **b.** qRT-PCR analysis of MTF1 and FDX1 expression in KIRC tissues and paired healthy tissues. **c**. Expression of MTF1 and FDX1 was confirmed by qRT-PCR in KIRC cell lines transfected with si-NC, siMTF1#1, and si-MTF1#2 or si-NC, siFDX1#1, and si-FDX1#2 in 786-O cells. **d.** CCK8 assay of cell proliferation capacity of 786-O cells after transfection with si-NC and si-MTF1#2 or si-NC and si-FDX1#2. **e.** EdU assay of cell proliferation capacity of 786-O cells after transfection with si-NC and si-MTF1#2 or si-NC and si-FDX1#2. **f**. Wound healing assay of cell proliferation capacity of 786-O cells after transfection with si-NC and si-MTF1#2 or si-NC and si-FDX1#2. (*p < 0.05, **p < 0.01, ***p < 0.001).

lipid acylated components of the tricarboxylic acid cycle, which in turn causes aggregation of lipid acylated proteins and loss of Fe-S cluster proteins, ultimately leading to cell death. The findings of Tsvetkov et al. [20] has led researchers to increasingly focus on the role of cuproptosis in the prognosis of patients with various tumors.

Acta
Materia
Medica

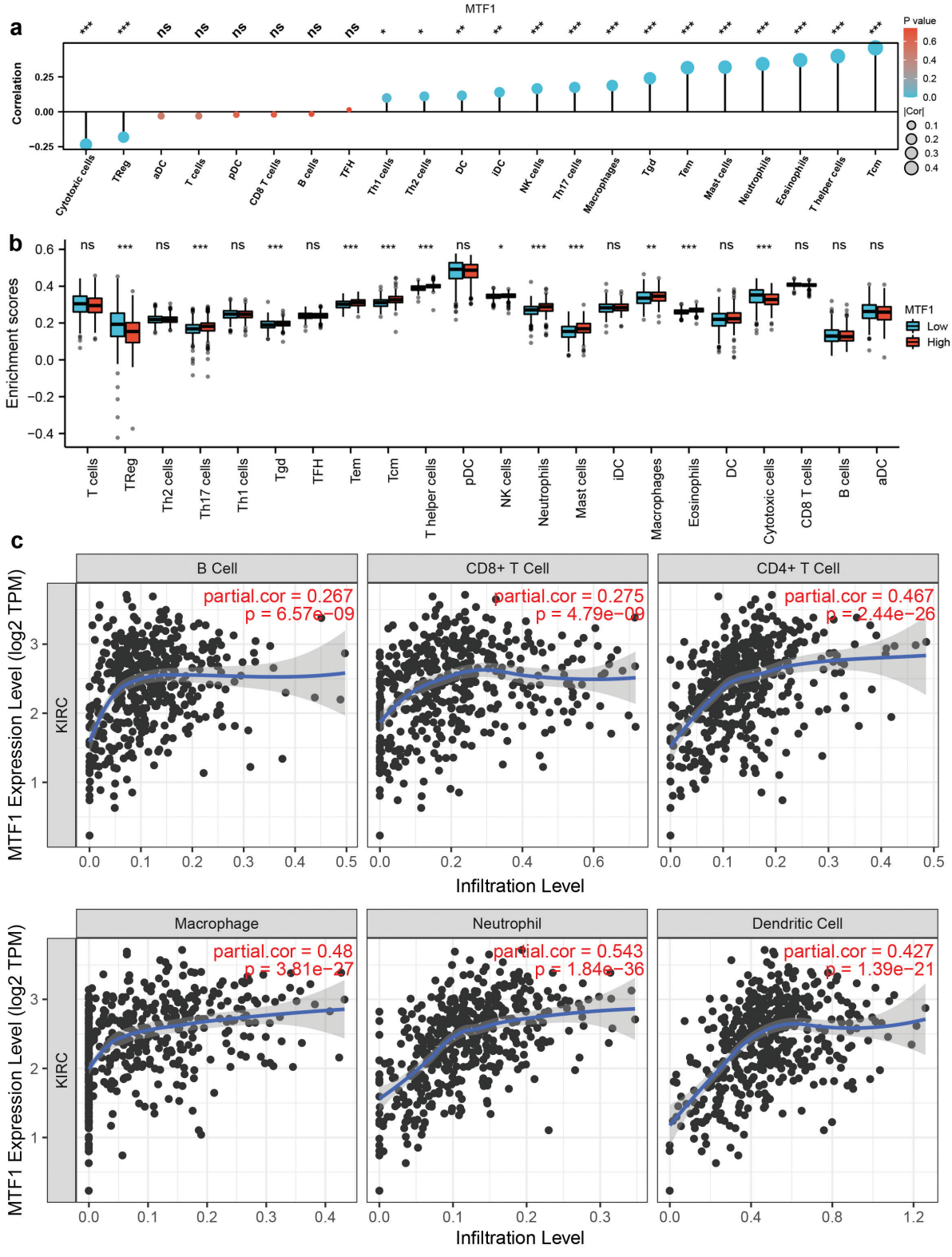

Figure 5 | MTF1 levels positively correlated with immune cell infiltration.
a. The relationship between MTF1 expression and 22 types of immune cells in KIRC. **b.** The level of 22 immune cell species expression in the high and low MTF1 groups. **c.** Relationship between MTF1 and B cells, CD8+ T cells, CD4+ T cells, macrophages, neutrophils, and dendritic cells using TIMER software.

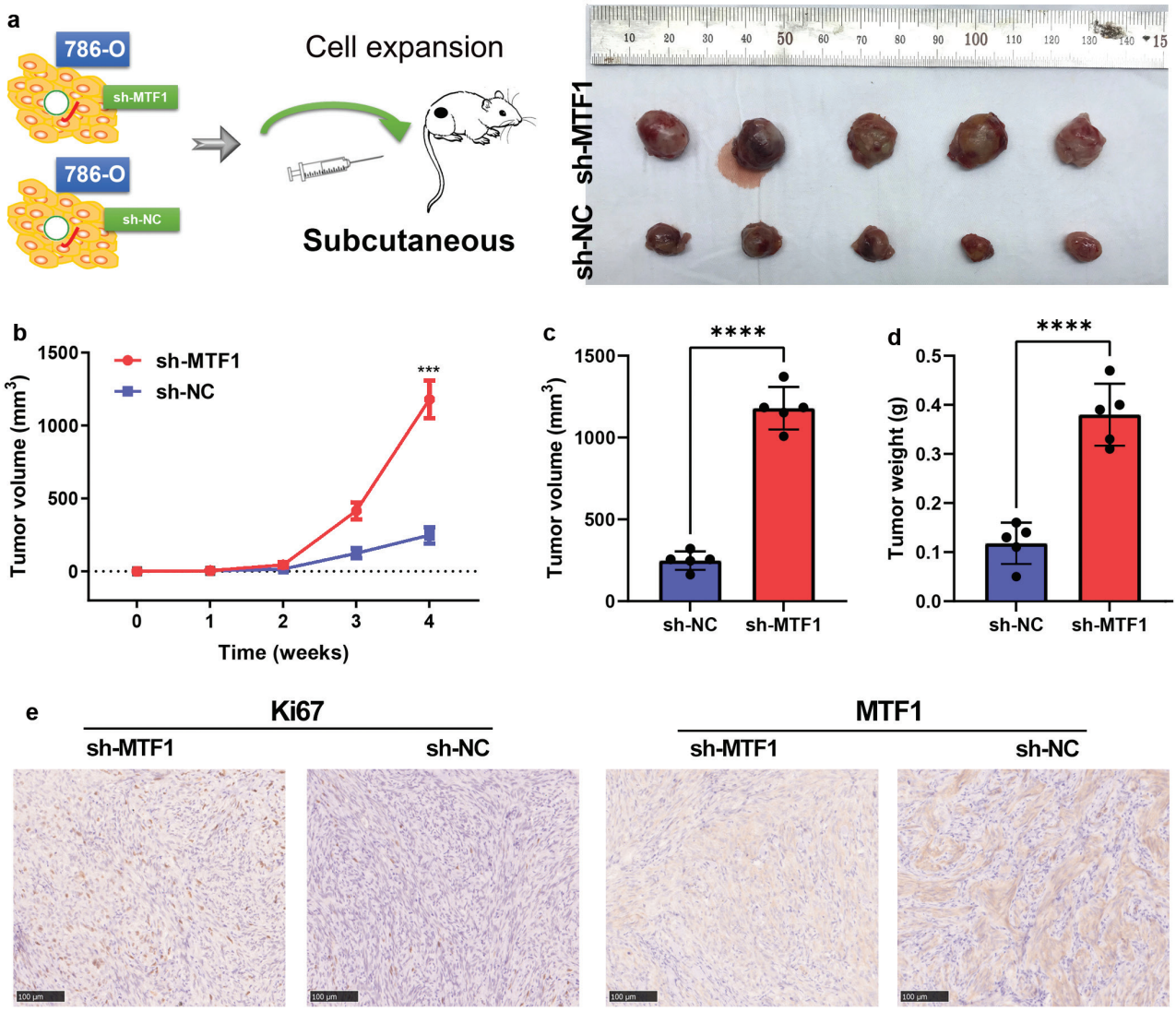

Figure 6 | Knockdown of MTF1 promotes tumor growth *in vivo*.
a. Representative images of subcutaneous xenograft model of sh-NC and sh-MTF1. **b-d**. Tumor growth curve (**b**), tumor weight (**c**), and tumor volume (**d**) in the subcutaneous xenograft model. **e.** Representative IHC images of ki67 and MTF1 for subcutaneous xenograft model. (***p < 0.001, ****p < 0.0001).

MTF1, located on chromosome 1p34.3, is a unique Cys2His2 zinc finger protein [14, 21]. MTF1 serves as a gene encoding a transcription factor that induces the regulation of metallothionein expression and other genes in response to heavy metals, including zinc, copper, and silver [22, 23]. MTF1 protein structure contains six highly-conserved zinc finger structural domains that regulate transcriptional activity by sensing and binding free zinc ions and DNA in the cell [24]. MTF1 is activated by heavy metals, cytokines, growth factors, and redox responses, and has an important role in metal homeostasis, embryogenesis, and hematopoiesis [25]. Previous studies have shown that MTF1 is aberrantly expressed in lung, cervical, breast, and colorectal cancers [25-27]. MTF1 expression in human KIRC has not been reported. Our study showed that MTF1, as an important CRG, has downregulated expression in KIRC and knockdown of MTF1 enhances KIRC proliferation and migration.

FDX1 is located on chromosome 11q23.3 and belongs to the Fe-S protein family, which is widely expressed in tissues associated with steroidogenesis [28, 29]. FDX1 encodes a small Fe-S protein that is involved in bile acid, vitamin D, and steroid metabolism by transferring electrons from NADPH to mitochondrial cytochrome P450 via ferro oxygenase reductase [30, 31]. It has been shown that loss of FDX1 function disrupts Fe-S clusterase activity and the homeostatic distribution of iron in cells, leading to mitochondrial iron overload and iron deficiency in the cytoplasm [32]. In contrast, there is an imbalance in iron homeostasis and increased Fe-S cluster

transport in tumor cells, which can lead to cancer cell proliferation, tumor growth, and metastasis [33, 34].

In conclusion, we screened four CRGs using the TCGA-KIRC dataset and constructed prognostic nomograms that accurately predicted OS in KIRC patients. In addition, MTF1 and FDX1 were identified as independent biomarkers of KIRC based on multivariate logistic regression analysis, and functional experiments revealed that knockdown of MTF1 and FDX1 expression promoted the migration and proliferation ability of KIRC. MTF1 acts as a tumor suppressor involved in the progression of KIRC by promoting proliferation and regulating immune cell infiltration.

ACKNOWLEDGEMENTS

The authors thank Biobank of Zhongda Hospital for providing tissue samples. This work was supported by Jiangsu Provincial Key Research and Development Program (BE2019751), and Jiangsu Provincial Medical Key Discipline (ZDXK202220).

CONFLICTS OF INTEREST

The authors declare that they have no competing interests.

REFERENCES

[1] Sung H, Ferlay J, Siegel RL, Laversanne M, Soerjomataram I, Jemal A, et al.: Global Cancer Statistics 2020: GLOBOCAN Estimates of Incidence and Mortality Worldwide for 36 Cancers in 185 Countries. *CA: A Cancer Journal for Clinicians* 2021, 71:209–249.

[2] Mao W, Wang K, Xu B, Zhang H, Sun S, Hu Q, et al.: ciRS-7 is a Prognostic Biomarker and Potential Gene Therapy Target for Renal Cell Carcinoma. *Molecular Cancer* 2021, 20:142.

[3] Chowdhury N, Drake CG: Kidney Cancer: An Overview of Current Therapeutic Approaches. *The Urologic Clinics of North America* 2020, 47:419–431.

[4] Powles T, Staehler M, Ljungberg B, Bensalah K, Canfield SE, Dabestani S, et al.: Updated EAU Guidelines for Clear Cell Renal Cancer Patients Who Fail VEGF Targeted Therapy. *European Urology* 2016, 69:4–6.

[5] Bedke J, Albiges L, Capitanio U, Giles RH, Hora M, Lam TB, et al.: The 2021 Updated European Association of Urology Guidelines on Renal Cell Carcinoma: Immune Checkpoint Inhibitor-based Combination Therapies for Treatment-Naive Metastatic Clear-Cell Renal Cell Carcinoma are Standard of Care. *European Urology* 2021, 80:393–397.

[6] Mao W, Wang K, Wu Z, Xu B, Chen M: Current Status of Research on Exosomes in General, and for the Diagnosis and Treatment of Kidney Cancer in Particular. *Journal of Experimental & Clinical Cancer Research* 2021, 40:305.

[7] Broadley M, Brown P, Çakmak İ, Rengel Z, Zhao F-J: Function of Nutrients: Micronutrient's. Marschner's Mineral Nutrition of Higher Plants (Third Edition), 2011. 191–248.

[8] Jaishankar M, Tseten T, Anbalagan N, Mathew BB, Beeregowda KN: Toxicity, Mechanism and Health Effects of Some Heavy Metals. *Interdisciplinary Toxicology* 2014, 7:60–72.

[9] Ge EJ, Bush AI, Casini A, Cobine PA, Cross JR, DeNicola GM, et al.: Connecting Copper and Cancer: From Transition Metal Signalling to Metalloplasia. *Nature Reviews, Cancer* 2022, 22:102–113.

[10] Cobine PA, Moore SA, Leary SC: Getting out What You Put in: Copper in Mitochondria and its Impacts on Human Disease. *Biochimica et Biophysica Acta - Molecular Cell Research* 2021, 1868:118867.

[11] Oliveri V: Selective Targeting of Cancer Cells by Copper Ionophores: An Overview. *Frontiers in Molecular Biosciences* 2022, 9:841814.

[12] Tsvetkov P, Coy S, Petrova B, Dreishpoon M, Verma A, Abdusamad M, et al.: Copper Induces Cell Death by Targeting Lipoylated TCA Cycle Proteins. *Science* 2022, 375:1254–1261.

[13] Westin G, Schaffner W: A Zinc-Responsive Factor Interacts with a Metal-Regulated Enhancer Element (MRE) of the Mouse Metallothionein-I Gene. *The EMBO Journal* 1988, 7:3763–3770.

[14] Brugnera E, Georgiev O, Radtke F, Heuchel R, Baker E, Sutherland GR, et al.: Cloning, Chromosomal Mapping and Characterization of the Human Metal-Regulatory Transcription Factor MTF-1. *Nucleic Acids Research* 1994, 22:3167–3173.

[15] Wiegand A, Meier W, Sutter E, Magalhães AC, Becker K, Roos M, et al.: Protective Effect of Different Tetrafluorides on Erosion of Pellicle-Free and Pellicle-Covered Enamel and Dentine. *Caries Research* 2008, 42:247–254.

[16] He J, Jiang X, Yu M, Wang P, Fu L, Zhang G, et al.: MTF1 has the Potential as a Diagnostic and Prognostic Marker for Gastric Cancer and is Associated with Good Prognosis. *Clinical and Translational Oncology* 2023, 24:1–11.

[17] Yang Y, Qian Cai Q, Sheng Fu L, Wei Dong Y, Fan F, Zhong Wu X: Reduced N6-Methyladenosine Mediated by METTL3 Acetylation Promotes MTF1 Expression and Hepatocellular Carcinoma Cell Growth. *Chemistry & Biodiversity* 2022, 19:e202200333.

[18] Obst JK, Mawji NR, Teskey SJL, Wang J, Sadar MD: Differential Gene Expression Profiles between N-Terminal Domain and Ligand-Binding Domain Inhibitors of Androgen Receptor Reveal Ralaniten Induction of Metallothionein by a Mechanism Dependent on MTF1. *Cancers (Basel)* 2022, 14:386.

[19] Wang K, Gu Y, Ni J, Zhang H, Wang Y, Zhang Y, et al.: Noncoding-RNA Mediated High Expression of Zinc Finger Protein 268 Suppresses Clear Cell Renal Cell Carcinoma Progression by Promoting Apoptosis and Regulating Immune Cell Infiltration. *Bioengineered* 2022, 13:10467–10481.

[20] Tang D, Chen X, Kroemer G: Cuproptosis: A Copper-Triggered Modality of Mitochondrial Cell Death. *Cell Research* 2022, 32:417–418.

[21] McLaughlin KA, Fairbank JA, Gruber MJ, Jones RT, Lakoma MD, Pfefferbaum B, et al.: Serious Emotional Disturbance among Youths Exposed to Hurricane Katrina 2 Years Postdisaster. *Journal of the American Academy of Child and Adolescent Psychiatry* 2009, 48:1069–1078.

[22] Balesaria S, Ramesh B, McArdle H, Bayele HK, Srai SK: Divalent Metal-Dependent Regulation of Hepcidin Expression by MTF-1. *FEBS Letters* 2010, 584:719–725.

[23] Adams SV, Barrick B, Christopher EP, Shafer MM, Makar KW, Song X, et al.: Genetic Variation in Metallothionein and Metal-Regulatory Transcription Factor 1 in Relation to Urinary Cadmium, Copper, and Zinc. *Toxicology and Applied Pharmacology* 2015, 289:381–388.

[24] He X, Ma Q: Induction of Metallothionein I by Arsenic via Metal-Activated Transcription Factor 1: Critical Role of C-terminal Cysteine Residues in Arsenic Sensing. *The Journal of Biological Chemistry* 2009, 284:12609–12621.
[25] Shi Y, Amin K, Sato BG, Samuelsson SJ, Sambucetti L, Haroon ZA, et al.: The Metal-Responsive Transcription Factor-1 Protein is Elevated in Human Tumors. *Cancer Biology & Therapy* 2010, 9:469–476.
[26] Giurato G, Nassa G, Salvati A, Alexandrova E, Rizzo F, Nyman TA, et al.: Quantitative Mapping of RNA-Mediated Nuclear Estrogen Receptor β Interactome in Human Breast Cancer Cells. *Scientific Data* 2018, 5:180031.
[27] Datta J, Majumder S, Kutay H, Motiwala T, Frankel W, Costa R, et al.: Metallothionein Expression is Suppressed in Primary Human Hepatocellular Carcinomas and is Mediated through Inactivation of CCAAT/Enhancer Binding Protein Alpha by Phosphatidylinositol 3-Kinase Signaling Cascade. *Cancer Research* 2007, 67:2736–2746.
[28] Sheftel AD, Stehling O, Pierik AJ, Elsässer HP, Mühlenhoff U, Webert H, et al.: Humans Possess Two Mitochondrial Ferredoxins, Fdx1 and Fdx2, with Distinct Roles in Steroidogenesis, heme, and Fe/S Cluster Biosynthesis. *Proceedings of the National Academy of Sciences of the United States of America* 2010, 107:11775–11780.
[29] Cai K, Tonelli M, Frederick RO, Markley JL: Human Mitochondrial Ferredoxin 1 (FDX1) and Ferredoxin 2 (FDX2) Both Bind Cysteine Desulfurase and Donate Electrons for Iron-Sulfur Cluster Biosynthesis. *Biochemistry* 2017, 56:487–499.
[30] Pechurskaya TA, Harnastai IN, Grabovec IP, Gilep AA, Usanov SA: Adrenodoxin Supports Reactions Catalyzed by Microsomal Steroidogenic Cytochrome P450s. *Biochemical and Biophysical Research Communications* 2007, 353:598–604.
[31] Hanukoglu I: Antioxidant Protective Mechanisms against Reactive Oxygen Species (ROS) Generated by Mitochondrial P450 Systems in Steroidogenic Cells. *Drug Metabolism Reviews* 2006, 38:171–196.
[32] Shi Y, Ghosh M, Kovtunovych G, Crooks DR, Rouault TA: Both Human Ferredoxins 1 and 2 and Ferredoxin Reductase are Important for Iron-Sulfur Cluster Biogenesis. *Biochimica et Biophysica Acta* 2012, 1823:484–492.
[33] Drakesmith H, Prentice A: Viral Infection and Iron Metabolism. *Nature Reviews, Microbiology* 2008, 6:541–552.
[34] Vernis L, El Banna N, Baille D, Hatem E, Heneman A, Huang ME: Fe-S Clusters Emerging as Targets of Therapeutic Drugs. *Oxidative Medicine and Cellular Longevity* 2017, 2017:3647657.